Astron. Astrophys. 329, 1045–1058 (1998)

ASTRONOMY
AND
ASTROPHYSICS

Photospheric metals in hot DA white dwarfs⋆

B. Wolff[1], **D. Koester**[1], **S. Dreizler**[2], **and S. Haas**[3]

[1] Institut für Theoretische Physik und Astrophysik, Universität Kiel, D-24098 Kiel, Germany (koester,wolff@astrophysik.uni-kiel.de)
[2] Institut für Astronomie und Astrophysik, Universität Tübingen, D-72076 Tübingen, Germany (dreizler@astro.uni-tuebingen.de)
[3] Dr.-Remeis-Sternwarte, Universität Erlangen-Nürnberg, Sternwartstr. 7, D-96049 Bamberg, Germany
(ai18@a400.sternwarte.uni-erlangen.de)

Received 21 July 1997 / Accepted 9 September 1997

Abstract. Previous observations of the soft X-ray and EUV region with the Einstein, EXOSAT, and ROSAT satellites have indicated the presence of photospheric absorbers in most DA white dwarfs with $T_{\rm eff} \gtrsim 40000$ K. Several of these objects have now been observed with the Extreme Ultraviolet Explorer (EUVE). Since the detection of individual metal lines is rather difficult with EUVE spectra we chose the well studied DA G 191-B2B as reference object for the analysis of other white dwarfs. In spectra obtained with the GHRS of the Hubble Space Telescope photospheric lines of nitrogen, silicon, iron, and nickel could be detected. With the abundances determined from these observations we were able to reproduce the EUVE spectrum of G 191-B2B. The main source of EUV opacity turned out to be iron, followed by nickel. The analysis of both the EUV continuum and the hydrogen Balmer lines led to $T_{\rm eff} = 56000 \pm 2000$ K. For the analysis of other DA white dwarfs we used the same relative abundances as for G 191-B2B but introduced a free scaling factor ("metallicity") for the total amount of metals. From EUVE spectra we determined relative metallicities for 20 objects with $T_{\rm eff} \gtrsim 40000$ K. The main result is that all DAs with $T_{\rm eff} \gtrsim 50000$ K contain additional photospheric absorbers, whereas at lower temperatures all observations, with the exception of GD 394, are compatible with pure hydrogen atmospheres. As in the case of G 191-B2B, iron determines also the EUV opacity in the objects at $T_{\rm eff} \gtrsim 50000$ K. This is in agreement with radiative levitation theory which predicts the support of iron above this temperature.

Key words: white dwarfs – stars: abundances – stars: atmospheres – ultraviolet: stars

1. Introduction

Observations of DA white dwarfs in the optical part of the electromagnetic spectrum result in the simple picture that the atmospheres consist completely of hydrogen. First hints for the presence of heavier elements came from observations in the UV region: Bruhweiler & Kondo (1981) detected CIV, NV, and SiIV lines in IUE spectra of G 191-B2B. However, it was very difficult to determine whether these features are of photospheric, circumstellar, or interstellar origin. Although the photospheric nature could be established with the detection of an H_α emission core having the same Doppler-shift as the IUE lines (Reid & Wegner 1988) the application of UV observations for the detection of metals in other white dwarfs is limited to a small number of bright objects.

More sensitive to traces of elements heavier than hydrogen are the X-ray and EUV regions of the electromagnetic spectrum. Photometric measurements with the Einstein (Kahn et al. 1984, Petre et al. 1986) and EXOSAT (Jordan et al. 1987, Paerels & Heise 1989) satellites showed that the X-ray/EUV fluxes of several hot DA white dwarfs were lower than predicted from pure hydrogen atmospheres. This result was first interpreted in the framework of hydrogen/helium atmospheres, either homogeneously mixed or chemically stratified. The photometric data could be explained by both hypotheses (Koester 1989, Vennes & Fontaine 1992). The only exception was the EXOSAT spectrum of Feige 24 which required a mixture of metals (Vennes et al. 1989).

A breakthrough for the explanation of the EUV flux deficit came with the observations of the ROSAT satellite. Barstow et al. (1993) demonstrated that the absorbing element in many DA white dwarfs could not be helium. Furthermore, the large number of white dwarfs detected in the ROSAT PSPC/WFC photometric survey allowed the determination of clear temperature limits (Barstow et al. 1993, Jordan et al. 1994, Jordan et al. 1996, Wolff et al. 1996, Marsh et al. 1997): all DA white dwarfs with effective temperatures below ≈ 40000 K do not contain significant amounts of photospheric absorbers whereas at $T_{\rm eff} \gtrsim 50000$ K most observations were incompatible with the assumption of pure hydrogen atmospheres. In the intermediate temperature range objects with pure hydrogen atmospheres and objects with additional absorbers could be found.

The generally accepted explanation for the presence of traces of heavier elements in white dwarf photospheres is ra-

Send offprint requests to: B. Wolff

⋆ Based on observations with the HST and EUVE satellites, and on optical spectra obtained at the DSAZ Calar Alto

diative levitation. Theoretical calculations (e.g. Vauclair et al. 1979, Chayer et al. 1995a) have shown that metals can be radiatively supported and prevented from sinking downwards at some effective temperatures and gravities. The presence of a temperature limit as derived from EUV observations implies that the absorbing elements can only be radiatively supported at $T_{\rm eff} \gtrsim 40000$ K. For a detailed comparison with theoretical predictions it is necessary to identify the elements present, which is not possible with the broad band photometry of the ROSAT survey.

A better tool for the detection of metals is provided by spectroscopic observations with the Extreme Ultraviolet Explorer (EUVE). Finley (1996, from broad band EUVE photometry) and Barstow et al. (1997a) could show that objects with additional absorbers are a distinct minority at $T_{\rm eff} \approx 40000$–$50000$ K. Although the spectral resolution is much improved compared to ROSAT, it is still very difficult to identify individual elements on the basis of EUV observations alone (e.g. Jordan et al. 1997a). This problem can be circumvented in the few cases where detections of photospheric metals are available from UV observations. In the case of G 191-B2B it could be demonstrated that the absorption features in the UV and EUV are largely caused by the same elements (Koester 1996, Barstow et al. 1996a, Lanz et al. 1996, Koester et al. 1997, Wolff et al. 1997).

In this paper we analyze optical, UV, and EUV observations of G 191-B2B to achieve a consistent fit for all spectral regions. We determine metal abundances from HST GHRS spectra and use these values for a fit of the EUVE spectrum. Effective temperatures are derived from optical and EUV observations. In the remainder of the paper we use the results for G 191-B2B to analyze the EUVE spectra of other DA white dwarfs.

2. Analysis of the DA white dwarf G 191-B2B

For the analysis of G 191-B2B we use three optical spectra obtained at the Calar Alto Observatory, observations with the Goddard High Resolution Spectrograph (GHRS) on the Hubble Space Telescope (HST) from Vidal-Madjar et al. (1994), and observations with the Extreme Ultraviolet Explorer. The primary aim of the GHRS observations was a study of the interstellar medium. Besides some interstellar features photospheric lines of NV, SiIV, FeV, and NiV could also be identified. For a detailed description we refer to Vidal-Madjar et al. (1994).

The EUVE spectra were obtained from the public archive. We use three dithered observations with a total exposure time of about 100000 seconds. In Table 2 a detailed list of all EUVE observations used in this paper can be found. The spectra were reduced (including flux calibration and subtraction of higher order contributions) with the standard procedures of the IRAF/EUV software package (Version 1.6.2).

All observations were analyzed with LTE as well as with non-LTE model atmospheres. Both models contain several millions of metal lines from the Kurucz lists on CD-ROM (Kurucz 1991) and bound-free opacities from the TOPBASE data base (Opacity Project, Cunto & Mendoza 1992, Seaton et al. 1992).

Table 1. Photospheric metal abundances in G 191-B2B as derived from UV observations. The predictions from radiative levitation theory for $T_{\rm eff} = 56000$ K and $\log g = 7.5$ are taken from calculations considering the effects of a fixed mixture of heavy elements on the atmospheric structure (Chayer et al. 1995b). As a comparison, we also list the results of the analysis of IUE spectra with non-LTE models by Lanz et al. (1996)

El.	Best fit	Low. limit	Up. limit	Pred.	Lanz96
C/H	$2 \cdot 10^{-6}$	$1 \cdot 10^{-6}$	$3 \cdot 10^{-6}$	$3 \cdot 10^{-6}$	$2 \cdot 10^{-6}$
N/H	$4 \cdot 10^{-6}$	$2 \cdot 10^{-6}$	$6 \cdot 10^{-6}$	$5 \cdot 10^{-6}$	$2 \cdot 10^{-7}$
Si/H	$1 \cdot 10^{-6}$	$6 \cdot 10^{-7}$	$2 \cdot 10^{-6}$	$3 \cdot 10^{-8}$	$3 \cdot 10^{-7}$
Fe/H	$5 \cdot 10^{-6}$	$2 \cdot 10^{-6}$	$1 \cdot 10^{-5}$	$5 \cdot 10^{-6}$	$1 \cdot 10^{-5}$
Ni/H	$1 \cdot 10^{-6}$	$8 \cdot 10^{-7}$	$2 \cdot 10^{-6}$		$2 \cdot 10^{-6}$

A description of the basic methods can be found in the papers of Koester (1996) and Werner & Dreizler (1997).

As a first step we analyzed the optical and ultraviolet spectra with LTE model atmospheres without considering the blanketing effect by metals. From a fit to the Balmer lines H_β, H_γ, and H_δ we determined $T_{\rm eff} = 60800$ K and $\log g = 7.59$. For the analysis of the HST observations we fixed effective temperature and gravity at these values and derived abundances for nitrogen, silicon, iron, and nickel by fitting the respective absorption lines. Since it is our aim to use the UV abundances for the interpretation of the EUVE spectrum we need the description of absorbing metals to be as complete as possible. Therefore, we determined also the carbon abundance from the equivalent width of the CIV doublet (1548/1550 Å, Bruhweiler & Kondo 1981) and added an oxygen abundance of O/H = $1 \cdot 10^6$ as given by Vennes et al. (1996b) and Lanz et al. (1996). However, it turned out later that these elements are rather unimportant for the EUV.

For the EUV analysis the synthetic spectra were normalized to the visual magnitude and the interstellar absorption was calculated with the IRAF/EUV package according to the model of Rumph et al. (1994). The values for the hydrogen and helium column densities (N(HI) = $2.07 \cdot 10^{18}$ cm^{-2}, HeI/HI = 0.072) were taken from Dupuis et al. (1995). We fixed the abundances at the values from the UV, calculated fully metal-blanketed atmospheres, and fitted the EUVE spectrum by varying only the effective temperature. This procedure resulted in a good fit at $T_{\rm eff} = 56000$ K.

It is not surprising that the effective temperature from the EUV spectrum is lower than the optical value derived with pure hydrogen atmospheres since the blanketing effect by absorption in the EUV changes the Balmer profiles so that an analysis with pure hydrogen models gives higher temperatures. This has been demonstrated by Bergeron et al. (1994) in the case of H+He atmospheres. We discuss the effects of the EUV absorption on the optical spectrum later in this section.

For the second analysis of the HST spectra we chose $T_{\rm eff} = 56000$ K and calculated the atmospheric structure using the previously determined mixture of metals. The abundances were only varied for the calculation of the synthetic spectra. The new

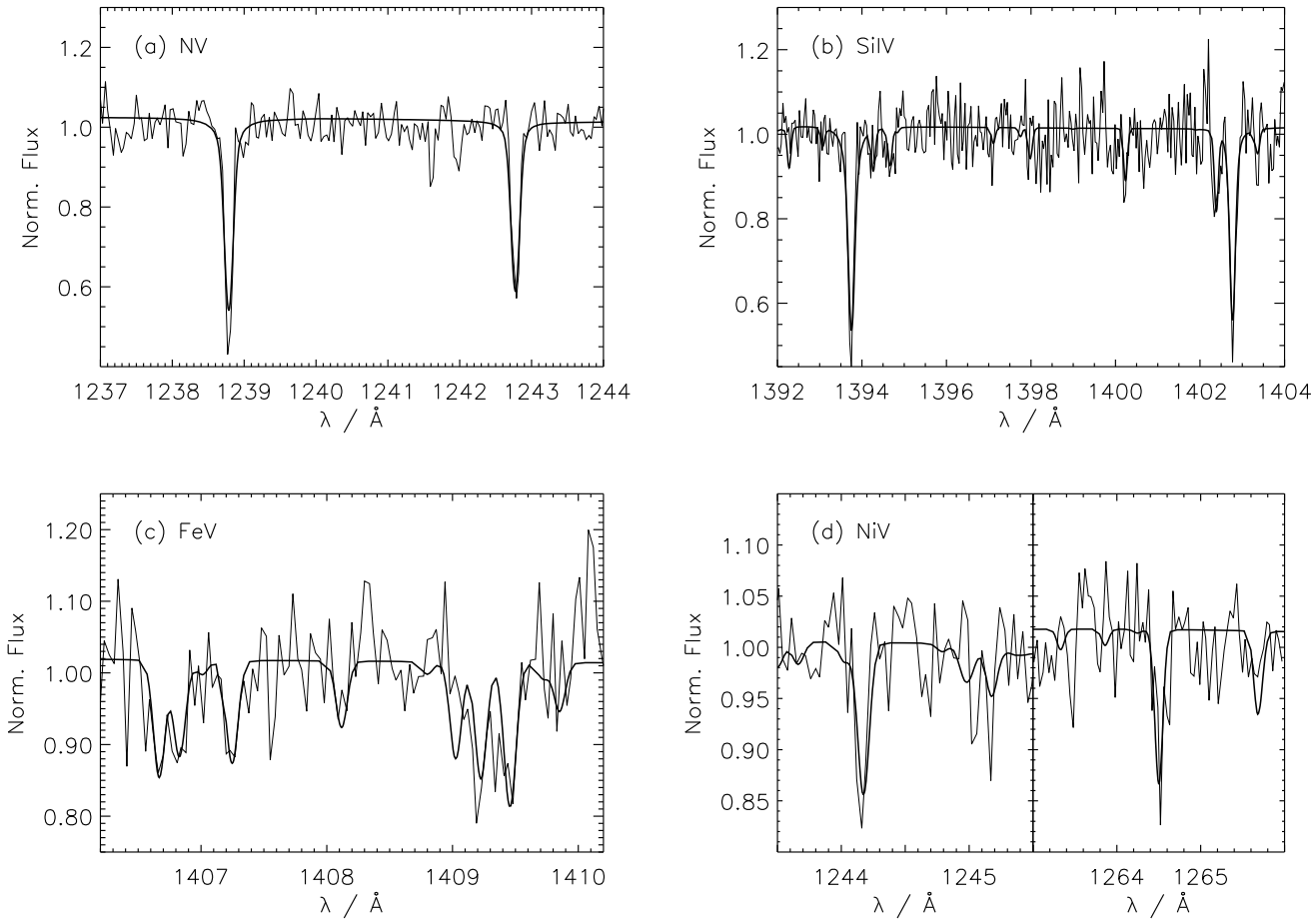

Fig. 1a–d. HST GHRS observations of G 191-B2B. **a** NV resonance lines compared to a fit with $N/H = 4 \cdot 10^{-6}$. **b** SiIV resonance lines compared to a fit with $Si/H = 1 \cdot 10^{-6}$. There are also several weak FeV lines visible. **c** FeV lines compared to a fit with $Fe/H = 5 \cdot 10^{-6}$. **d** NiV lines compared to a fit with $Ni/H = 1 \cdot 10^{-6}$

results are given in Table 1 and the fits to the UV lines are plotted in Fig. 1. A renewed calculation of the atmospheric structure using the metal mixture from Table 1 did not change the UV abundances significantly so that these values can be considered as the final results.

These observed abundances are compared with the predictions of diffusion theory (Chayer et al. 1995b). The results for carbon, nitrogen, and iron are in good agreement. For silicon our values are significantly higher than the prediction. This effect is also seen in several other DA white dwarfs with high temperatures (see Chayer et al. 1995a, Holberg et al. 1997, and references therein).

In Table 1 we also list the abundances obtained from an analysis of IUE spectra with non-LTE model atmospheres (Lanz et al. 1996). For the two most important elements – iron and nickel – the values from Lanz et al. (1996) agree within the error limits. Significant deviations can be seen for nitrogen and silicon.

With the new abundances the EUVE spectrum could also be reproduced at $T_{\rm eff}$ = 56000 K. As can be seen from Fig. 2a the agreement between the synthetic spectrum and the EUVE observation is remarkable good, considering the fact that only the effective temperature was varied. However, the synthetic flux near the maximum at about 250–290 Å is somewhat too low and at $\lambda \lesssim 230$ Å there seems to be some opacity missing. The fit near the maximum can be optimized if the metal abundances are reduced to the lower limits of the UV analysis (see Table 1) but then the discrepancy at shorter wavelengths becomes stronger (Fig. 2b).

Since this discrepancy appears just below the HeII ionization edge at 228 Å we have tested the possible influence of helium on the synthetic spectrum, which was also investigated by Lanz et al. (1996) and Wolff et al. (1997). In Fig. 2b the result with an interstellar HeII abundance of $HeII/HI = 0.2$ is also shown. It can be seen that HeII can contribute some of the required opacity, but the flux at very small wavelengths is still too high. A similar result can be obtained with a photospheric helium abundance of $He/H = 5 \cdot 10^{-5}$. Helium can also improve the fit if the original abundances from Table 1 are used. However, these results do not prove the presence of ionized interstellar or photospheric helium. At short wavelengths, there is a need of additional opacity, which can partly be provided by helium.

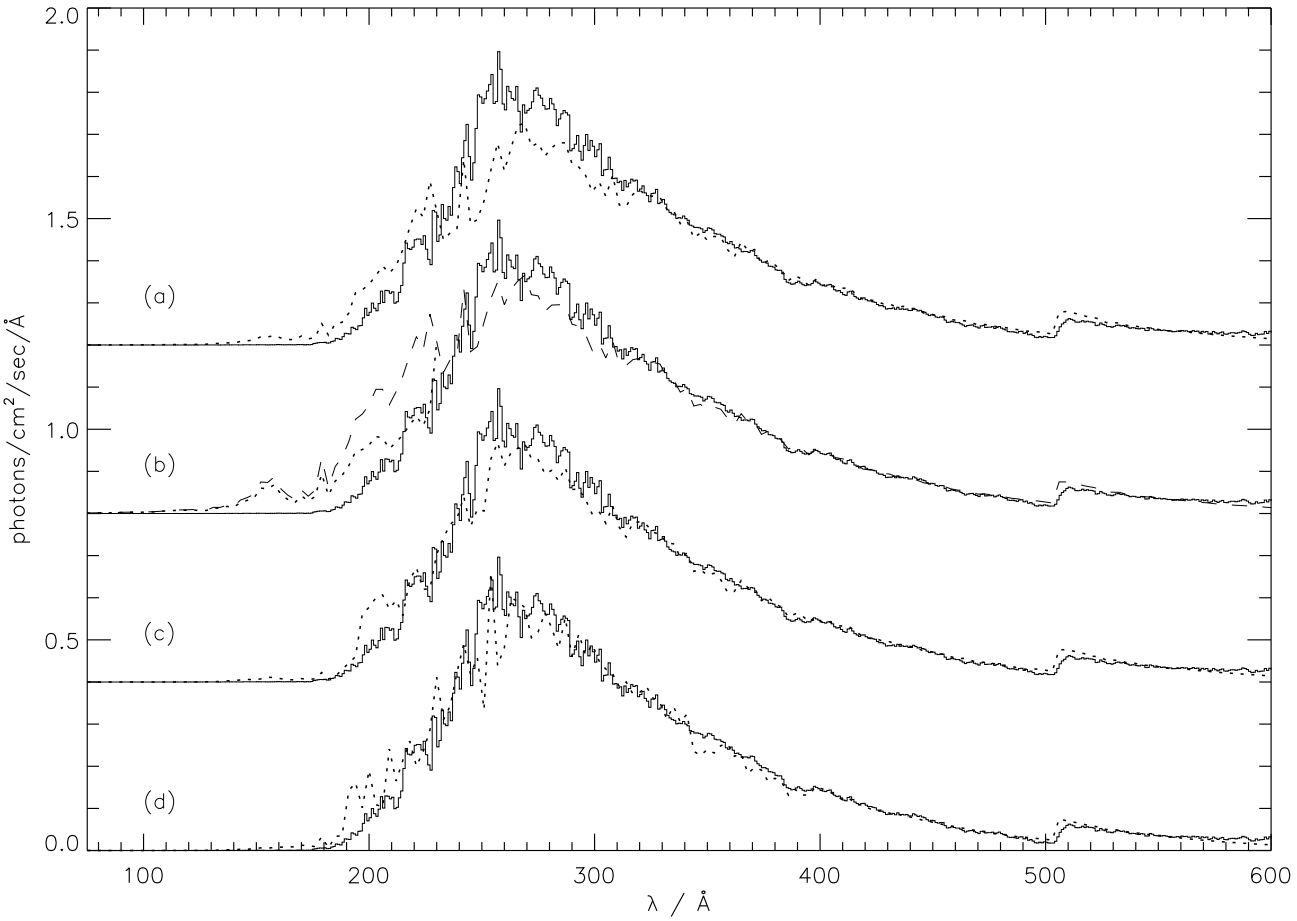

Fig. 2a–d. Fits to the EUVE spectrum of G 191-B2B (continuous line). The observed spectrum is flux calibrated and subtracted from higher order contributions. The individual spectra from the SW, MW, and LW spectrometers were concatinated at appropriate points to give a continious spectrum. All models have $T_{\rm eff}$ = 56000 K and $\log g$ = 7.6, the interstellar absorption is assumed to be N(HI) = $2.07 \cdot 10^{18}$ cm^{-2} and HeII/HI = 0.072. **a** LTE model with C/H = $2 \cdot 10^{-6}$, N/H = $4 \cdot 10^{-6}$, O/H = $1 \cdot 10^{-6}$, Si/H = $1 \cdot 10^{-6}$, Fe/H = $5 \cdot 10^{-6}$, Ni/H = $1 \cdot 10^{-6}$. **b** LTE model with C/H = $1 \cdot 10^{-6}$, N/H = $2 \cdot 10^{-6}$, O/H = $5 \cdot 10^{-7}$, Si/H = $6 \cdot 10^{-7}$, Fe/H = $2 \cdot 10^{-6}$, Ni/H = $8 \cdot 10^{-7}$, and HeII/HI = 0 (dashed line), or HeII/HI = 0.2 (dotted line), respectively. **c** Same as **b**, but with Ne/H = $1 \cdot 10^{-5}$ and HeII/HI = 0.15. **d** Non-LTE model with C/H = $2 \cdot 10^{-6}$, N/H = $4 \cdot 10^{-6}$, O/H = $1 \cdot 10^{-6}$, Si/H = $1 \cdot 10^{-6}$, Fe/H = $1 \cdot 10^{-5}$, Ni/H = $1 \cdot 10^{-6}$, and HeII/HI = 0.2

The given HeII/HI and He/H values should be regarded more as upper limits than as precise determinations.

In the following we discuss other possibilities to account for the missing opacity. Therefore, it is important to know that the shape of the model spectrum is dominated by iron with minor contributions from nickel. Both elements are responsible for the strong decrease in flux shortward of 250 Å. The most important ionization stages are FeV and NiV; FeVI and NiVI become important at $\lambda < 170$ Å. Other elements exhibit some strong lines but their contribution to the flux decrease is rather small.

It is not possible to increase the opacity at $\lambda < 250$ Å with the elements considered so far (C, N, O, Si, Fe, Ni) without getting too strong absorption features at longer wavelengths. Therefore, we investigated several other elements for their possible contributions to the opacity in the EUV region. The first candidates were phosphorus and sulphur. Both elements were detected in FUV spectra obtained with the ORFEUS telescope (Vennes et al. 1996b). The authors determined P/H = $2.5 \cdot 10^{-8}$ and S/H = $3.2 \cdot 10^{-7}$. Both abundances are far too low for detectable EUV features. The values had to be increased to more than $3 \cdot 10^{-6}$ for a contribution to the opacity below 230 Å. This is not only in contradiction with the FUV observations but these abundances would also result in detectable features at $\lambda > 250$ Å.

After having investigated all elements which were directly observed in spectra of G 191-B2B, we considered several other elements with high cosmic abundances: neon, sodium, magnesium, aluminium, argon, and calcium. The most promising candidates were neon, sodium, and magnesium. These elements have absorption edges from NeIII, NaIII, and MgIII at 200, 180, and 150 Å, respectively. In Fig. 2c we display a fit with Ne/H = $1 \cdot 10^{-5}$ and HeII/HI = 0.15. The flux shortward of 200 Å is almost completely absorbed whereas at longer wavelengths no additional features are visible. There are also no detectable lines in the ultraviolet and optical regions.

This result does not necessarily mean that there is indeed photospheric neon present in G 191-B2B since individual lines could not be identified. The predicted neon abundance of Ne/H = $1 \cdot 10^{-6}$ from Chayer et al. (1995b) is also lower than the value required for the EUV. However, neon (and sodium and magnesium) can in principle make an important contribution to the EUV opacity. The other elements considered (Al, Ar, Ca) can be excluded because the abundances needed for a contribution below 230 Å would give detectable features in the EUV at longer wavelengths.

There are also several other possibilities for the explanation of the flux deficit. The largest uncertainties arise from the atomic data which are partly inaccurate at EUV wavelengths. Pradhan (1996) remarked that the improved calculations by the Iron Project (Bautista et al. 1996) showed significant changes in opacity for FeV at $\lambda < 300$ Å compared to the Opacity Project calculations. The uncertainties for nickel, the second most important element in the EUV, are even larger, because detailed calculations are not yet available and, therefore, we had to use hydrogenic cross sections.

Besides uncertainties of atomic data, two assumptions made for the calculation of synthetic spectra may also affect our results: uniform distribution of trace elements and validity of LTE. Since the support of trace elements by radiative forces results in a non-uniform (stratified) distribution, the absorption features in the UV and EUV may differ in strength from uniform calculations. The influence of non-LTE effects is discussed later in this section.

We come now back to the determination of the effective temperature. The EUVE observations can be used to derive precisely $T_{\rm eff}$ if the wavelength region at $\lambda \gtrsim 300$ Å is used. In this part the absorption by heavy elements is rather small. If the metal abundances are high enough to account for the blanketing effect at $\lambda < 250$ Å then $T_{\rm eff}$ can be very well determined from the EUVE spectra. This determination is insensitive to the actual metal mixture if the abundances are varied within the error limits given by the HST analysis. So far, we have used the N(HI) determination of Dupuis et al. (1995). Our previous result ($T_{\rm eff}$ = 56000 K) is not changed significantly, if the interstellar column density is not fixed, because the region at $\lambda \gtrsim 300$ can be used to determine $T_{\rm eff}$ and N(HI) simultaneously. Important for the discussion below is, that the lower limit for the effective temperature is 54000 K, even if the column density is not fixed.

We started the analysis of G 191-B2B with a fit to the Balmer lines using pure hydrogen atmospheres. The result was $T_{\rm eff}$ = 60800 K. After the analysis of the UV and EUV spectra we reanalyzed the optical data using metal-blanketed atmospheres with abundances taken from Table 1. This resulted in an effective temperature of 50400 K, about 10000 K lower than the first determination and more than 5000 K lower than the EUV value. The discrepancy between the optical and EUV results could not be resolved if the abundances were changed to the lower boundaries of Table 1. In this case the Balmer lines gave $T_{\rm eff}$ = 51000 K. In order to obtain a temperature as high as the lower limit from the EUVE spectrum ($T_{\rm eff}$ = 54000 K) the iron abundance had to be changed to Fe/H = $5 \cdot 10^{-7}$. Of course, this abundances is incompatible with the HST observations and the flux decrease at $\lambda < 250$ Å cannot be reproduced either. A higher temperature from the analysis of the Balmer lines can only be achieved if the blanketing effect in the EUV can be reduced. But this is not possible since a significant amount of absorbing metals is necessary to reproduce the EUVE spectra.

The question is whether this discrepancy is due to the use of the LTE approximation. In order to examine this assumption we continued the analysis of G 191-B2B with non-LTE model atmospheres. As a first step we used the abundances from Table 1 for a fit of the EUVE spectrum. Again, the best solution is $T_{\rm eff}$ = 56000 K. Compared to the LTE model, the maximum at 250–290 Å is reproduced better. At lower wavelengths there is, as in the case of LTE models, some opacity missing. This region can be fitted better, if the iron abundance is increased to Fe/H = $1 \cdot 10^{-5}$ and an interstellar HeII abundance of HeII/HI = 0.2 is used (Fig. 2d).

For a test of non-LTE effects in the UV region we fitted the FeV lines again with non-LTE models. We restricted the investigation to iron since this element is most important in the EUV. The result is Fe/H = $(2 \,^{+\,3}_{-\,1}) \cdot 10^{-6}$, which is somewhat lower than the LTE value. Both values are compatible within the error margins. However, the low abundance from the non-LTE analysis is incompatible with the abundance of Fe/H = $1 \cdot 10^{-5}$ from the EUV fit. As in the LTE case, there is a need of additional opacity at short wavelengths.

After reproducing the EUVE spectrum with non-LTE models we analyzed the hydrogen Balmer lines again. We used the abundances from Table 1 with the exception of iron for which we used Fe/H = $1 \cdot 10^{-5}$ to account for the required EUV opacity. We determined $T_{\rm eff}$ = 54200 K and $\log g$ = 7.46. Now, the temperatures from EUV and optical spectra are in agreement. A similar result using non-LTE models has also been found by Lanz et al. (1996).

Summarizing, we have found a solution for the EUVE spectrum of G 191-B2B with the use of LTE and non-LTE model atmospheres. These results are in agreement with the abundances derived from HST GHRS observations and in the case of non-LTE models also with the temperature determined from hydrogen Balmer lines. In the next paragraph we will use our knowledge about G 191-B2B to understand the EUVE spectra of other DA white dwarfs.

3. EUVE spectra of other DA white dwarfs

We have obtained spectra of 20 DA white dwarfs from the EUVE public archive. A description of the observations can be found in Table 2. All stars are in the temperature region at $T_{\rm eff} \gtrsim 40000$ K where the ROSAT observations implied the presence of photospheric metals. As in the case of G 191-B2B we reduced the data using standard procedures of the IRAF/EUV package to obtain flux calibrated spectra (photons $\rm cm^{-2} s^{-1} Å^{-1}$). The individual spectra from the SW, MW, and LW EUVE spectrometers were concatinated.

In Fig. 3–6 we display the EUVE spectra of our sample. The maximum flux of each spectrum is normalized to unity

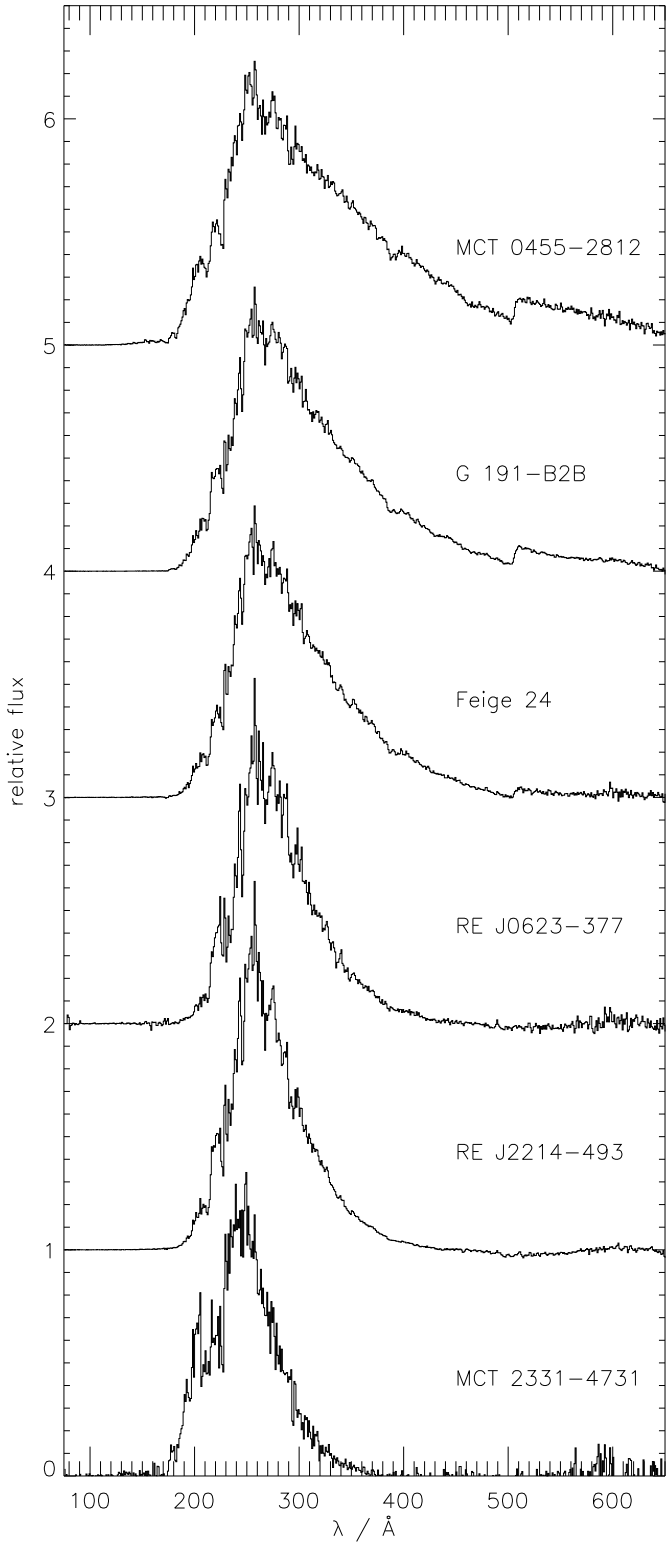

Fig. 3. EUVE spectra of the G 191-B2B group

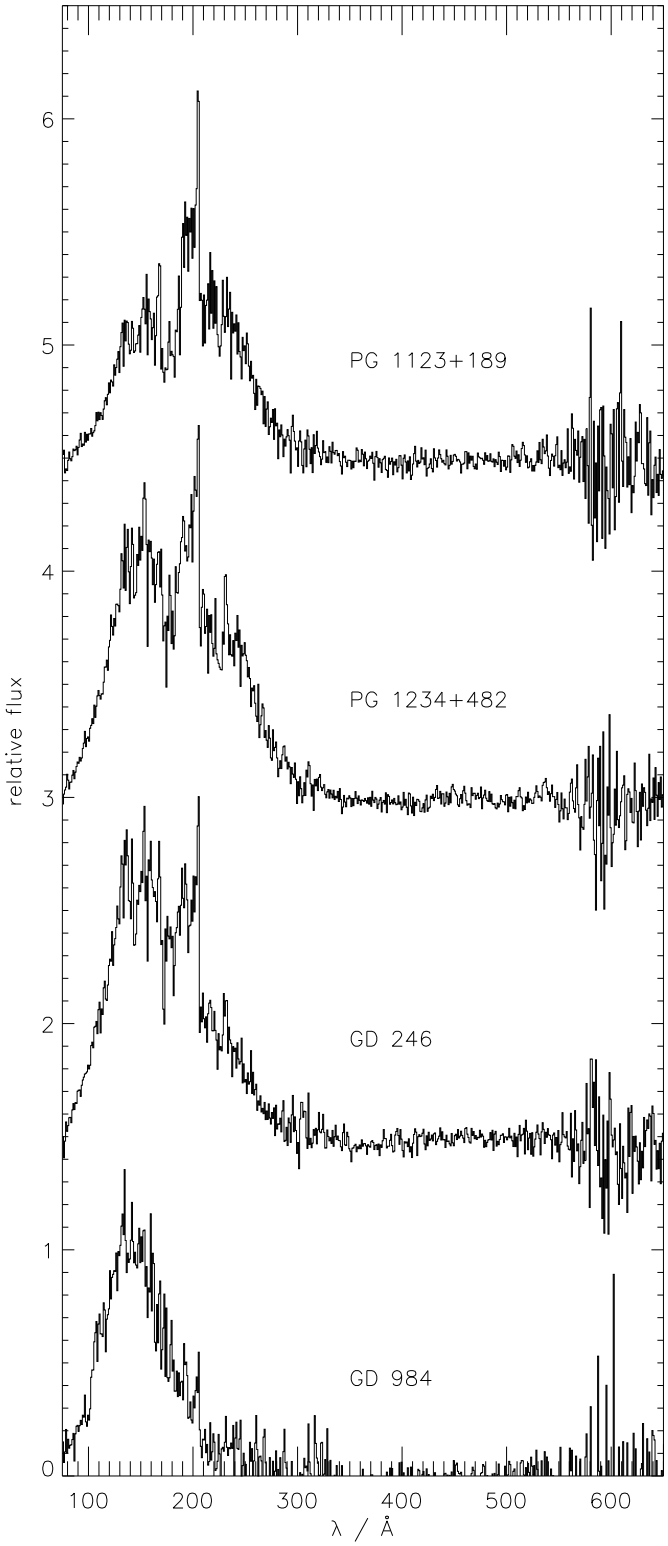

Fig. 4. EUVE spectra of the GD 246 group

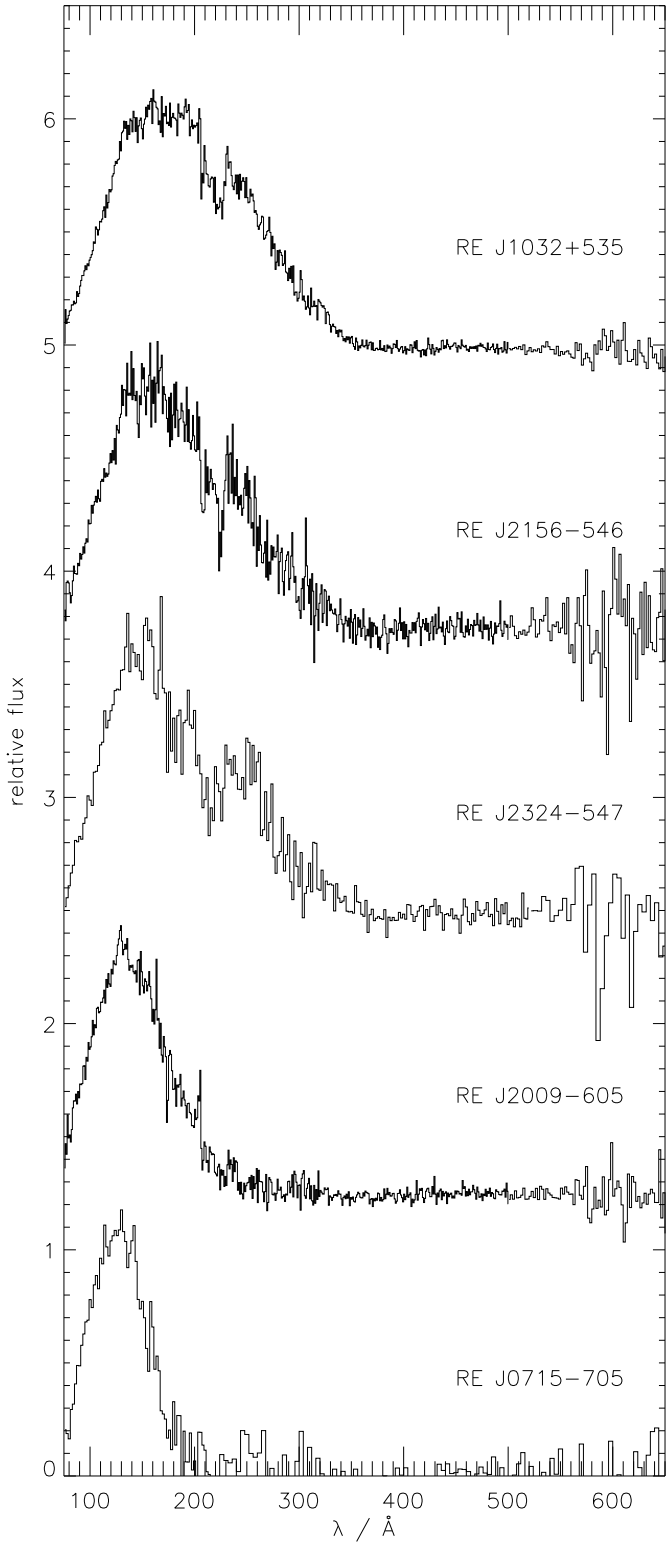

Fig. 5. EUVE spectra of white dwarfs with pure hydrogen atmospheres

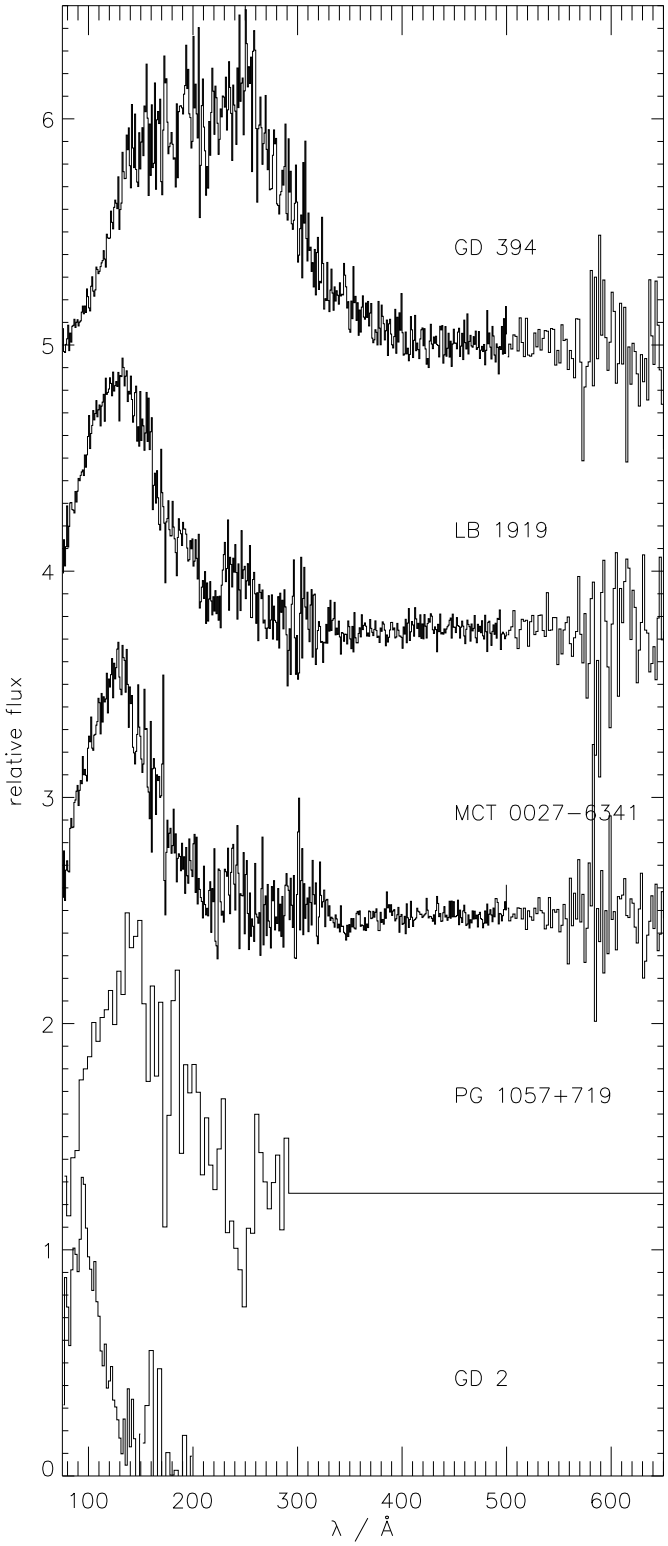

Fig. 6. EUVE spectra different from the types presented in Fig. 3–5

Table 2. List of EUVE observations used in this paper

Object	Observation dates	Exp. times for SW, MW, and LW [ksec]
LB 1919	1994/04/16–04/22	166.4, 165.8, 163.0
RE J2214−493	1994/08/12–08/17	125.0, 116.9, 122.3
MCT 0027−6341	1994/09/07–09/11	104.4, 105.0, 98.2
Feige 24	1993/11/25–11/26	26.4, 25.5, 24.5
	1994/10/22–10/23	25.6, 25.6, 24.2
	1995/01/22–01/24	25.1, 23.0, 21.6
	1995/10/31–11/01	31.5, 29.2, 27.5
G 191-B2B	1993/10/28–10/30	53.2, 47.8, 50.4
	1993/12/07–12/08	26.1, 20.1, 24.2
	1994/03/05–03/08	45.8, 43.7, 44.1
GD 246	1994/07/16–07/17	35.0, 34.9, 32.2
	1994/08/08	14.0, 13.2, 13.4
RE J0623−377	1993/11/23–11/24	35.4, 35.8, 33.6
PG 1234+482	1996/03/07–03/10	67.2, 65.8, 65.6
	1996/03/12–03/16	130.4, 130.8, 127.3
MCT 2331−4731	1993/08/08–08/10	56.5, 54.0, 54.5
MCT 0455−2812	1993/11/14–11/16	55.6, 48.4, 52.5
PG 1123+189	1995/03/13–03/19	201.5, 198.8, 190.8
GD 984	1995/08/23–08/26	91.8, 84.3, 86.6
	1995/08/26–08/30	97.3, 87.9, 89.9
	1995/08/30–08/31	41.8, 40.2, 38.2
GD 2	1993/10/19–10/20	50.6, 47.5, 48.2
RE J1032+535	1995/04/07–04/10	97.5, 92.4, 94.6
	1995/04/10–04/14	101.3, 94.9, 96.8
	1995/04/14–04/15	31.5, 30.0, 29.4
RE J2324−547	1995/07/29–08/02	87.2, 87.4, 80.6
	1995/08/02–08/05	89.2, 89.9, 84.3
RE J2156−546	1995/07/24–07/27	95.1, 94.4, 87.5
	1995/07/27–07/29	54.0, 53.8, 49.7
RE J2009−605	1994/07/09–07/13	106.5, 102.9, 101.8
RE J0715−705	1995/09/02–12/02	77.0, 76.2, 71.8
PG 1057+719	1994/01/05–01/07	58.5, 57.1, 55.9
	1994/02/21–02/22	57.1, 56.4, 55.1
GD 394	1993/09/13–09/16	47.1, 46.7, 50.0

to facilitate the comparison of different objects. The stars are divided into four groups according to the overall shape of the spectra. The first group (Fig. 3) consists of white dwarfs similar to G 191-B2B. All spectra have a maximum flux around 250 Å and a sharp decrease at shorter wavelenghts. The differences appear mainly at the long-wavelength tail and are caused by different interstellar absorption. Our conclusion from this figure is that the photospheric absorbers in these objects are largely the same.

For the second group (Fig. 4) GD 246 can be taken as prototype. The flux at $\lambda \gtrsim 300$ Å is completely absorbed and the maximum is shifted towards 150–200 Å. There are two reasons which can explain the differences compared to the G 191-B2B group. From the missing long-wavelength tail it can be concluded that the interstellar hydrogen column density must be higher towards the GD 246 objects. The second reason can be seen directly from a comparison of MCT 2331−4731 with GD 246. Both stars have about the same effective temperatures and visual magnitudes, and the maximum flux is ≈ 0.015 photons $\mathrm{cm}^{-2}\mathrm{s}^{-1}\mathrm{Å}^{-1}$ in both cases. However, the spectrum of MCT 2331−4731 shows a strong decrease shortward of ≈ 200 Å where GD 246 has its maximum. The only explanation for this behaviour is that GD 246 contains less photospheric metals than MCT 2331−4731.

To support the conclusion that all objects from the second group have lower abundances than G 191-B2B, we have used the observed EUVE spectrum of G 191-B2B and calculated a spectrum without interstellar absorption by applying the model of Rumph et al. (1994) with negative column densities ("dereddening"). For this purpose we have used the column densities of our EUVE fit ($N(\mathrm{HI}) = 2.07 \cdot 10^{18}\,\mathrm{cm}^{-2}$, HeI/HI = 0.072, HeII/HI = 0.0). The largest uncertanties arise from the HeII density which cannot be determined exactly from the G 191-B2B analysis, but a change from HeII/HI = 0.0 to 0.2 does not influence our conclusion.

With this dereddened spectrum we have tried to fit the spectra of the GD 246 group by adjusting interstellar absorption and a free scaling factor. The scaling factor is necessary to account for different visual magnitudes and effective temperatures. We were only able to reproduce the region at $\lambda > 250$ Å. At shorter wavelengths the G 191-B2B flux rapidly reaches zero. It is not possible to shift the maximum flux of the G 191-B2B spectrum towards shorter wavelengths by increasing interstellar absorption because the long-wavelength part of the observed spectrum can not be reproduced with higher column densities.

We have also used this method to investigate the G 191-B2B group itself. The result is that the spectra are indeed very similar. The deviations from the prototype are only small: The heavy element abundances seem to be somewhat higher in RE J0623−377 and RE J2214−493, and somewhat lower in MCT 0455−2812 and MCT 2331−4731.

Besides the objects of the GD 246 group there are several other white dwarfs with even lower abundances. These objects are presented in Fig. 5. Finally, in Fig. 6 we have collected all objects which cannot be classified by their spectra in a simple way.

After this phenomenologic analysis we have investigated the EUVE spectra in a more quantitative way. Our approach is to take G 191-B2B as reference object. We assume that the elements and their relative abundances are the same as in the prototype (see Table 1). To account for different amounts of absorbers we introduce a scaling factor ("metallicity") for the total abundance of all elements. This factor can be defined as $m = n_{\mathrm{obs}}/n_{\mathrm{G191}}$ where n_{obs} is the total abundance of heavy elements determined by a fit to the EUVE spectrum of the star and n_{G191} is the value for G 191-B2B.

The use of a metallicity index has several advantages. It simplifies the analysis of EUVE spectra since individual element abundances have not to be considered. This makes it possible to investigate a large number of DA white dwarfs without getting the difficulties described in the analysis of G 191-B2B and to compare directly the amount of heavy elements in these stars.

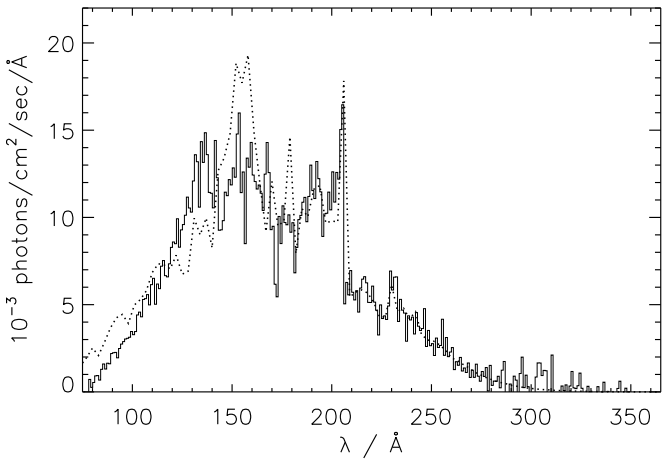

Fig. 7. Fit to the EUVE spectrum of GD 246 with $T_{\rm eff}$ = 59000 K, $\log g$ = 7.8, m = 0.25, N(HI) = $1.6 \cdot 10^{19}$ cm^{-2}, HeI/HI = 0.07, and HeII/HI = 0.025

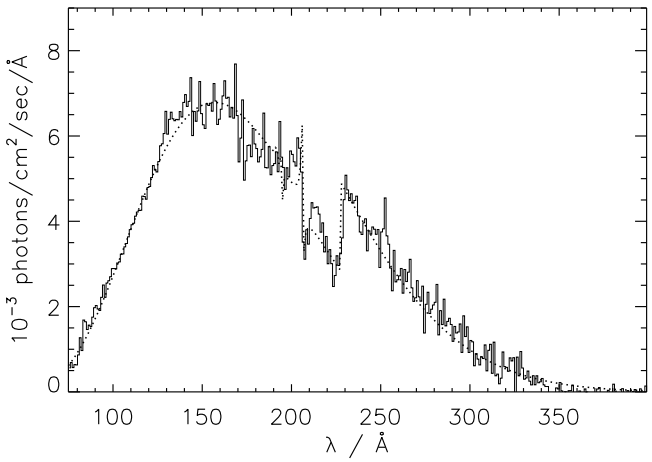

Fig. 8. Fit to the EUVE spectrum of RE J2156−547 with a pure hydrogen atmosphere and $T_{\rm eff}$ = 44000 K, $\log g$ = 7.9, N(HI) = $7.0 \cdot 10^{18}$ cm^{-2}, HeI/HI = 0.065, HeII/HI = 0.05

The use of a reference object also enables us to analyze the majority of objects where it is not possible to determine element abundances from UV spectra. The determination of individual abundances in these objects would be almost impossible with EUVE spectra alone.

The main assumption in adopting a metallicity index is that the relative abundances are the same as in the prototpye. This also implies that the EUV opacity is mainly provided by iron with smaller contributions from nickel. This can be justified in case of the G 191-B2B group because all EUVE spectra of this group are very similar. Such a justification does not exist for the other groups. For some objects, we discuss the validity of this assumption later in this paper.

From the definition of the metallicity it is clear that abundances of individual elements cannot be determined with our method. One exception may be the iron abundance since this element dominates the EUV opacity and the metallicity is mainly a measure of this abundance.

In contrast to the analysis of G 191-B2B it is, in general, not possible to consider the effective temperature as a free parameter. The reason is that the determination of $T_{\rm eff}$ rests on the long-wavelength tail of the EUVE spectrum. For many stars the interstellar absorption is so strong that this tail is only partly visible. In this case changes of $T_{\rm eff}$ can be compensated by changes in metallicity and N(HI). Therefore, we fixed effective temperature (and gravity) at the optically determined values (taken from Finley et al. 1997).

Interstellar features of HeI and HeII are visible in several spectra allowing the determination of HeI/HI and HeII/HI ratios together with hydrogen column densities. In those cases where these features could not be detected we have used mean values of HeI/HI = 0.07 and HeII/HI = 0.02 for the fit. In Table 3 we list the results of our analysis.

The determination of metallicities confirms the picture we have drawn from the simple investigation of the spectra. All white dwarfs in the G 191-B2B group have metallicities comparable to or up to a factor of four higher than the prototype. This is in agreement with previous analyses of UV spectra (Holberg et al. 1993, 1994; Werner & Dreizler 1994), showing that the abundances of iron and nickel in RE J0623−377 and RE J2214−493 are higher than in Feige 24 and G 191-B2B. The stars in the GD 246 group have significantly lower metallicities of 20%–40% of the G 191-B2B value. In the third group all stars are compatible with pure hydrogen atmospheres. As examples we present two fits to EUVE spectra in Fig. 7 and 8.

The stars in the fourth group show a small range of metallicities. Two of them, GD 2 and PG 1057+719, are largely compatible with pure hydrogen atmospheres. They could be classed with the third group. MCT 0027−6341 is a white dwarf with a high temperature and comparitively low abundances. The metallicity is similar to the GD 246 group but the temperature is somewhat higher. Another object with high $T_{\rm eff}$ is LB 1919 (WD 1056+516). Finley et al. (1997) could not determine the effective temperature because the flat-bottomed line profiles indicated high rotational velocities. If we use the temperature given by Vennes et al. (1997) ($T_{\rm eff}$ = 68600 K) then the metallicity would be $m \approx 0.1$ so that LB 1919 may be similar to MCT 0027−6341. The last object of the fourth group is GD 394. For $T_{\rm eff}$ = 39600 K we determined a metallicity of 25 %. Since the temperature of GD 394 is rather low we do not class this object with the GD 246 group and discuss it in detail in Sect. 4.

We have to make some remarks on the interpretation of the metallicities. Our method uses the UV abundances of G 191-B2B as reference values. As discussed in Sect. 2 these abundances cannot perfectly reproduce the EUVE spectrum. This fact is rather unimportant in the case of the other stars of the G 191-B2B group since these objects can be reproduced equally well with the G 191-B2B abundances or with higher values. It is decisive for the interpretation of the metallicities of the GD 246 group. As can be seen from Fig. 2a the observed spectrum of G 191-B2B cannot be reproduced at $\lambda \lesssim 200$ Å because the synthetic flux is too high at this region. Unfortunately, the max-

Table 3. Results of the analysis of the EUVE spectra. For each star we list the optically determined effective temperature and gravity from Finley et al. (1997), the temperature used for the fit, and the fit results metallicity m and interstellar column densities

WD Number	Name	opt. $T_{\rm eff}$ / K	$\log g$	used $T_{\rm eff}$ / K	m	N(HI) [10^{18} cm^{-2}]	HeI/HI	HeII/HI
1056+516	LB 1919			69000[a]	0.1	16.0	0.07	0.06
2211−495	RE J2214−493	66100	7.38	66000	4.0	5.8	0.07	≤ 0.05
0027−636	MCT 0027−6341	63700	7.96	64000	0.2	27.5	0.06	0.02
0232+035	Feige 24	62700	7.17	62000	1.0	3.25	0.05	≤ 0.2
				60000	1.0	3.0	0.05	≤ 0.2
0501+527	G 191-B2B	61200	7.49	56000	1.0	2.0	0.07	≤ 0.2
2309+105	GD 246	58700	7.81	59000	0.25	16.0	0.07	0.025
0621−376	RE J0623−377	58200	7.27	58000	2.0	5.0	0.07	≤ 0.1
1234+482	PG 1234+482	56400	7.67	56000	0.2	13.0	0.065	0.03
2331−475	MCT 2331−4731	55800	8.07	56000	0.75–1.0	8.5	≤ 0.07	0.05–0.1
0455−282	MCT 0455−2812	55700	7.77	66000	1.0	1.3	0.075	≤ 0.15
1123+189	PG 1123+189	53800	7.63	54000	0.4	12.5	0.085	0.025
0131−164	GD 984	50000	7.67	50000	0.2	22.0	0.075	0.03
0004+330	GD 2	49400	7.63	49000	≤ 0.1	110.0	0.07	0.02
1029+537	RE J1032+535	46900	7.77	47000	≤ 0.05	7.5	0.055	0.045
				44000	0.0	5.5	0.07	0.06
2321−549	RE J2324−547	45000	7.94	45000	0.05	9.5	0.07	0.08
				42000	0.0	8.5	0.07	0.07
2152−548	RE J2156−546	44300	7.91	44000	0.0	7.0	0.065	0.05
2004−605	RE J2009−605	44200[b]	8.14	44000	≤ 0.025	17.5	0.07	0.025
		41900[c]	8.16	42000	0.0	16.5	0.07	0.02
0715−703	RE J0715−705	43900	8.05	44000	0.0	26.0	0.07	0.02
1057+719	PG 1057+719	41500	7.90	41500	0.1	27.5	0.07	0.0
2111+498	GD 394	39600	7.94	39600	0.25	6.5	0.07	0.07

[a] see text; [b] Marsh et al. (1997); [c] Vennes et al. (1996a)

imum flux of GD 246 is in this region making a comparison of GD 246 with G 191-B2B rather difficult. However, this uncertainty influences only the value of the metallicity of GD 246 relative to G 191-B2B since the EUV spectrum of GD 246 can be fitted well with the adopted abundances. The value of 25 % from our analysis can be considered as an upper limit for the real relative metallicity because the photospheric opacity of G 191-B2B at $\lambda \lesssim 200$ Å must be higher than the opacity used for our analysis.

This conclusion is supported if we take the improved abundances used for Fig. 2c for a fit of the GD 246 spectrum. Then, the abundances of GD 246 would be about 15 % of the G 191-B2B values. It may be argued that it would be better to use these improved abundances in general, but then the fit at short wavelengths is determined mainly by neon. Since it is not certain that neon is actually present in G 191-B2B and other DA white dwarfs a fit with neon is not more valuable than without this element. The main problem in comparing GD 246 with G 191-B2B is that we cannot say exactly which elements are responsible for the absorption at $\lambda \lesssim 200$ Å.

Regardless of this discussion, one main result of our analysis is that the element abundances of the GD 246 group must be lower than the values of the G 191-B2B group. As pointed out in Sect. 2 iron and nickel are most important for the opacity in the EUV. This means that we measure mainly the abundances of these elements if we determine the metallicity with our method. Therefore, we conclude that iron and nickel are less abundant in GD 246 than in G 191-B2B. However, it is not plausible that they are absent in GD 246. The EUVE spectrum can be reproduced without iron and nickel, but then the abundances of carbon, nitrogen, oxygen, and silicon have to be increased to about three times the G 191-B2B values. These values are significantly higher than the upper limits from IUE observations as determined by Vennes et al. (1991): $\mathrm{C/H} \leq 5 \cdot 10^{-7}$, $\mathrm{N/H} \leq 3.2 \cdot 10^{-6}$, and $\mathrm{Si/H} \leq 3.2 \cdot 10^{-8}$. Therefore, a significant contribution of iron and nickel to the EUV opacity seems to be necessary. A similar result was also found by Jordan et al. (1997a, b) from an analysis of the GD 246 group star PG 1234+482.

A comparison of our abundances from the fit with m = 0.25 with the values from Vennes et al. shows that carbon and nitrogen are compatible with these upper limits whereas the silicon abundance of $\mathrm{Si/H} = 2.5 \cdot 10^{-7}$ is too high. Since silicon does not contribute to the EUV opacity, it is also possible to reproduce the GD 246 spectrum with a lower silicon abundance. The upper limit from Vennes et al. does not affect our solution for the metallicity of GD 246.

As in the analysis of G 191-B2B, we also tested the influence of non-LTE effects on our results. The observed spectra of the G 191-B2B group can be reproduced as well as in the LTE case if the iron abundance is doubled as in the non-LTE analysis of G 191-B2B itself. The metallicities are again in the range m = 1–4. For the GD 246 group the abundances have to be around 30 % of the values needed for the EUV fit of G 191-B2B, in agreement with the results from the LTE analysis. However, the fits for the GD 246 group are slightly worse compared to the LTE case. The reason for this behaviour is a change of the ionization equilibria for iron: In the LTE case FeV is far more abundant than FeVI whereas in non-LTE both ions are approximately equal by abundance. This is important only at $\lambda < 200$ Å because of strong absorption features of FeVI in this region.

4. Remarks on individual objects

MCT 0455−2812. Finley et al. (1997) determined $T_{\rm eff}$ = 55700 ± 600 K from a fit to the hydrogen Balmer lines. This is in contradiction with the result from the EUV analysis: The EUVE spectrum cannot be fitted with an effective temperature lower than 63000 K. Similar results were also obtained by Dupuis et al. (1995) and Barstow et al. (1997b). The latter authors fitted also the Lyman lines with $T_{\rm eff}$ = 66500 K.

RE J1032+535, RE J2324−547. There is weak evidence for photospheric metals at the optically determined temperatures of both stars. However, a fit with pure hydrogen atmospheres is possible in both cases, if the effective temperature is decreased by 3000 K. We think that the observational results are not sufficient to prove the existence of additional absorbers in these stars. Barstow et al. (1997a) have fitted the EUVE spectrum of RE J2324−547 with photospheric helium of He/H = $2 \cdot 10^{-5}$ or with a stratified hydrogen-helium atmosphere having $M_{\rm H}$ = $1.6 \cdot 10^{-13}\, M_\odot$. This does not rule out the possibility for photospheric metals since the deviations of the observed spectrum from pure hydrogen models appear at $\lambda < 150$ Å where the influence of helium is rather small.

PG 1057+719. Holberg et al. (1997) determined upper limits of C/H < $6.3 \cdot 10^{-9}$, N/H < $1.6 \cdot 10^{-6}$, and Si/H < $7.9 \cdot 10^{-10}$ from GHRS observations of PG 1057+719. These upper limits are compatible with the EUVE observations. If we use the optically determined temperature of 41500 K and the upper limits for C, N, and Si, the fit to the EUVE spectrum is somewhat better than with a pure hydrogen atmosphere.

GD 394. Photospheric lines of silicon can be observed in IUE and GHRS spectra of GD 394. Vennes et al. (1991) and Barstow et al. (1996b) have determined abundances of Si/H = $1.6 \cdot 10^{-6}$ and Si/H = $3 \cdot 10^{-6}$, respectively. Other elements could not be detected, but for carbon an upper limit of C/H < $3 \cdot 10^{-8}$ could be given. However, despite of the high silicon abundance, the EUV opacity cannot be provided by this element. Barstow et al. have fitted the EUVE spectrum mainly with nitrogen and oxygen at O/H = N/H = $2.5 \cdot 10^{-6}$. This value is similar to the upper limits for both elements so that the EUV fit is compatible with the UV observations. However, it cannot be proven that the EUV opacity is provided by nitrogen and oxygen alone. We were able to reproduce the EUVE spectrum of GD 394 mainly with an iron abundance of Fe/H = $1.25 \cdot 10^{-6}$, corresponding to a metallicity of m = 0.25 (see Fig. 9). This index would also imply a silicon abundance of Si/H = $2.5 \cdot 10^{-7}$ which is an order of magnitude lower than the UV value. Therefore, it is evident that the relative abundances of heavy elements in GD 394 are not the same as in G 191-B2B. Nevertheless, our solution demonstrates the possibility to fit the EUVE spectrum with iron and not with nitrogen and oxygen since silicon does not contribute significantly to the EUV opacity. With an abundance of Fe/H = $1.25 \cdot 10^{-6}$ the UV iron lines would not be stronger than ≈ 6 mÅ and would, therefore, not be detectable on existing spectra. It cannot be determined whether nitrogen, oxygen, iron, or a mixture of all three elements are the main contributions to the EUV opacity.

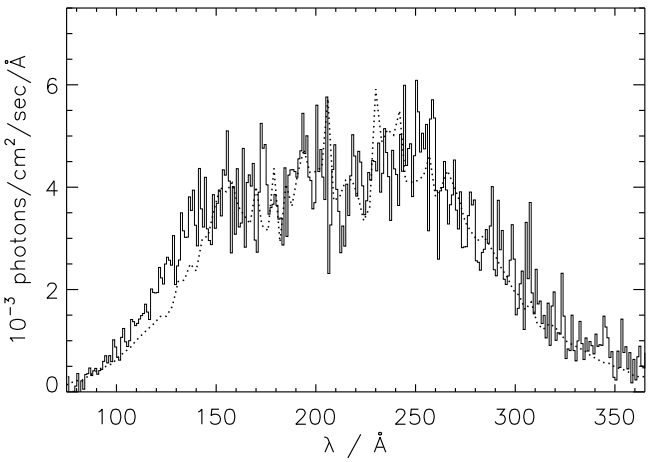

Fig. 9. Fit to the EUVE spectrum of GD 394 with $T_{\rm eff}$ = 39600 K, $\log g$ = 7.94, m = 0.25, N(HI) = $6.5 \cdot 10^{18}$ cm^{-2}, HeI/HI = 0.07, HeII/HI = 0.07

MCT 2331−4731. As in the case of G 191-B2B, the absorption features of the synthetic spectrum are somewhat too strong around 250 Å. A better fit can be achieved if neon is added and the abundances are reduced to 75 % of the values used for Fig. 2c. The EUVE spectrum of MCT 2331−4731 is the only spectrum of the G 191-B2B group where the HeII edge is clearly visible and the autoionization feature of HeI at 206 Å is indicated. The edge can be fitted with an interstellar density of N(HeII) = 4.24–8.5 · 10^{17} cm^{-2} (HeII/HI = 0.05–0.1). Alternatively, a photospheric abundance of He/H ≤ $3 \cdot 10^{-5}$ can be used. The exact values for HeII/HI and He/H depend strongly on the used chemical composition. For the same reason, only an upper limit of HeI/HI = 0.07 can be given for interstellar HeI.

5. Discussion

Our analysis of the EUVE spectra shows that several DA white dwarfs with $T_{\rm eff} \gtrsim 56000$ K can be reproduced with the same or higher abundances as in G 191-B2B. We have also found five objects with $T_{\rm eff} \gtrsim 50000$ K having lower abundances than G 191-B2B but still with significant amounts of photospheric metals. For this group GD 246 can be regarded as prototype. The main source of opacity in both the G 191-B2B and the GD 246 group is iron, followed by nickel. At lower temperatures absorption by metals is not detectable in virtually all white dwarfs: The observations are compatible with the assumption of pure hydrogen atmospheres. We did not find any object with a pure hydrogen atmosphere and a higher temperature than HZ 43A ($T_{\rm eff}$ = 50800 K, Finley et al. 1997), which was earlier found to contain only negliglible amounts of additional photospheric absorbers (e.g. Barstow et al. 1995). The only object showing clear detections of metals at lower temperatures is GD 394 with $T_{\rm eff}$ = 39600 K (see Sect. 4).

The basic explanation for the presence of traces of metals in the photospheres of hot DA white dwarfs is diffusion combined with radiative levitation. The abundances should be dependent on effective temperature and surface gravity. For example, the theory predicts that iron is more abundant at higher $T_{\rm eff}$ and lower $\log g$ (e.g. Chayer et al. 1995b). Also the existence of minimum temperatures for radiative support of iron are predicted. The observed distribution of metals should resemble these predictions. Therefore, it is an important question if there is a connection between GD 394 and the metal rich white dwarfs at $T_{\rm eff} \gtrsim 50000$ K. If there is a gap in the distribution of white dwarfs containing photospheric heavy elements between 40000 and 50000 K, then GD 394 would be an exceptional object and it would be likely that its EUV opacity is provided by other elements than in the objects at higher temperatures, where iron is dominant. Otherwise, it would be possible that iron is also important in GD 394 and that iron can be radiatively supported at $T_{\rm eff} \gtrsim 40000$ K.

Although the ROSAT all-sky survey implied the existence of metals in DA atmospheres at $T_{\rm eff} \approx$ 40000–50000 K, this result could not be confirmed with pointed EUVE observations. One reason may be that only few candidates for photospheric metals in this temperature range were observed during the EUVE Guest Observer Program. From the candidates for additional absorbers found by Wolff et al. (1996) only RE J2324−547 is in our sample. At the optically determined temperature of 45000 K there is indeed weak evidence for photospheric metals (m = 0.05). However, the EUVE spectrum can also be reproduced with a pure hydrogen atmosphere at $T_{\rm eff}$ = 42000 K.

Recently, Holberg et al. (1997) have found another object at low temperatures with photospheric metals. This star (RE J1614−085) has $T_{\rm eff}$ = 38500 K, and exhibits a significant EUV opacity in the ROSAT survey similar to GD 394 (Marsh et al. 1997, Holberg et al. 1997) but unlike GD 394 it is nitrogen and not silicon which is the most abundant element. Holberg et al. determined $\mathrm{C/H} = 5 \cdot 10^{-7}$, $\mathrm{N/H} = 2.5 \cdot 10^{-4}$, and $\mathrm{Si/H} = 1 \cdot 10^{-8}$ from HST GHRS observations. Important for our discussion is the fact that the chemical compositions of both stars are different although they have similar effective temperatures and gravities. This makes it likely that radiative levitation is not the dominant process determining photospheric abundances in these stars. Holberg et al. proposed strong mass loss or weak accretion to explain the different compositions of GD 394 and RE J1614−085 and to explain the deviations from radiative levitation theory. Together with the possible gap of photospheric metals at $T_{\rm eff} \approx$ 40000–50000 K, it is, therefore, also probable that the source of the EUV opacity in GD 394 is different from the metal rich objects at $T_{\rm eff} \gtrsim 50000$ K. In this case, the beginning of sufficient radiative support of iron would be seen at GD 984 with $T_{\rm eff} \approx 50000$ K. This would be in agreement with diffusion theory which predicts that iron can be radiatively supported above $T_{\rm eff} \approx$ 45000–50000 K at $\log g$ = 8.0 (Chayer et al. 1995b).

Another confirmation for radiative levitation theory would be an agreement between predicted and observed abundances. From our EUVE fits we determine mainly the iron abundance so that this value can be compared with the theory. In Fig. 10 we present a comparison with the predictions from Chayer et al. (1995b). We have plotted only the theoretical values for $\log g$ = 7.5 to keep the figure clear. In order to consider the effects of gravity we have corrected each observed abundance value so that the difference between observation and theory in the figure is equal to the difference for the real $\log g$ of the star.

Fig. 10 shows that the abundances of several stars from both the G 191-B2B and the GD 246 group are approximately compatible with the theoretical predictions. However, there are several stars with large deviations: GD 984 and MCT 2331−4731 have higher abundances whereas PG 1234+482 and Feige 24 have lower abundances than the predictions. The abundances for MCT 0455−2812 do agree if the effective temperature from our EUVE fit (66000 K) is used.

This comparison shows that there may be other important processes besides radiative levitation which determine the surface composition, a conclusion which was also found by Chayer et al. (1995a) from an investigation of abundance determinations with UV spectra. Another example can be found at $T_{\rm eff} \approx 50000$ K: GD 984 shows significant amounts of metals whereas GD 2 has a rather pure hydrogen atmosphere, and HZ 43 at a slightly higher gravity is the most prominent example of a pure hydrogen atmosphere. However, the predictions of the radiative levitation theory do agree with the observations at least for some stars of the G 191-B2B and GD 246 groups. Therefore, one may conclude that diffusion and levitation are not disturbed by other processes in these stars, whereas such processes may be active in other cases to provide lower or higher abundances for iron.

The nature of these mechanisms is puzzling. Chayer et al. (1997) have investigated the influence of constant mass loss and accretion on the silicon abundance in DA white dwarfs. They have found that strong mass loss or weak accretion may provide an overabundance of silicon, whereas mass loss at lower levels results in a photosphere depleted from silicon. Similar calculations for iron do not yet exist but it seems plausible that

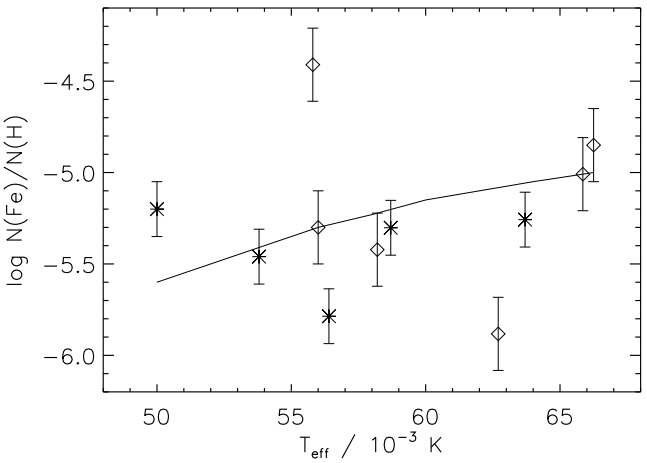

Fig. 10. Comparison of observed iron abundances with predictions from radiative levitation theory. The predictions (solid line) for $\log g = 7.5$ are taken from calculations considering the effects of a contaminated background plasma of heavy elements (Chayer et al. 1995b). The observed iron abundances are taken from our EUVE analysis with metallicities. Stars denote the GD 246 group (GD 984, PG 1123+189, PG1234+482, GD 246, and MCT 0027−6341) and diamonds the G 191-B2B group (MCT 2331−4731, RE J0623−377, G 191-B2B, Feige 24, MCT 0455−2812, and RE J2214−493, from left to right). Typical errors are ± 0.15 dex for the GD 246 group and ± 0.2 dex for the G 191-B2B group

the main results are the same. Within this scenario, overabundances of iron as in MCT 2331−4731 can be easily explained. Underabundances may be caused by weak mass loss. However, the mass loss rate must not be too strong so that iron does not disappear from the photosphere on evolutionary time scales.

There is one uncertainty which might strongly influence our conclusions. Chayer et al. (1995b) have used the TOPBASE data base which does not consider the fine structure of iron. As shown by Chayer et al. (1994), using data from Kurucz (1991), the predicted abundances may be eight times larger if the fine structure is not ignored. In this case, the iron abundance of most stars may be too low, and we need in almost every case mechanisms for the reduction of abundances.

Nevertheless, the EUVE observations have marked the beginning of radiative support of iron at $T_{\rm eff} \approx 50000$ K. This is a strong support for diffusion theory. For the distribution of iron in individual stars, it is, however, necessary to include additional mechanisms.

Acknowledgements. We would like to thank A. Vidal-Madjar for the contribution of the HST observations, S. Jordan for the EUVE spectrum of PG 1234+482, and H. Jessop and the EUVE staff for the immediate response to archive requests. We would also like to thank the referee J.B. Holberg for useful comments. This work has been supported by the Deutsche Agentur für Raumfahrtangelegenheiten (DARA) under grant 50 OR 96173. We have made use of the Simbad data base, operated at CDS, Strasbourg, France.

References

Barstow M.A., Fleming T.A., Diamond C.J., et al., 1993, MNRAS 264, 16
Barstow M.A., Holberg J.B., Koester D., 1995, MNRAS 274, L31
Barstow M.A., Hubeny I., Lanz T., Holberg J.B., Sion E.M., 1996a. In: Bowyer S., Malina R.F. (eds.), Astrophysics in the Extreme Ultraviolet, Kluwer, Dordrecht, p. 185
Barstow M.A., Holberg J.B., Hubeny I., et al., 1996b, MNRAS 279, 1120
Barstow M.A., Dobbie P.D., Holberg J.B., Hubeny I., Lanz T., 1997a, MNRAS 286, 58
Barstow M.A., Holberg J.B., Hubeny I., Lanz T., 1997b. In: Isern J., Hernanz M., Garcia-Berro E. (eds.), White Dwarfs, Kluwer, Dordrecht, p. 237
Bautista M.A., Nahar S.N., Peng J., Pradhan A.K., Zhang H.L., 1996. In:Bowyer S., Malina R.F. (eds.), Astrophysics in the Extreme Ultraviolet, Kluwer, Dordrecht, p. 577
Bergeron P., Wesemael F., Beauchamp A., et al., 1994, ApJ 432, 305
Bruhweiler F., Kondo Y., 1981, ApJ 248, L123
Chayer P., LeBlanc F., Fontaine G., et al., 1994, ApJ 436, L161
Chayer P., Fontaine G., Wesemael F., 1995a, ApJS 99, 189
Chayer P., Vennes S., Pradhan A.K., et al., 1995b, ApJ 454, 429
Chayer P., Fontaine G., Pelletier C., 1997. In: Isern J., Hernanz M., Garcia-Berro E. (eds.), White Dwarfs, Kluwer, Dordrecht, p. 253
Cunto W., Mendoza C., 1992, Rev.MexicanaAstron.Astrofiz., 23 107
Dupuis J., Vennes S., Bowyer S., Pradhan A.K., Thejll P., 1995, ApJ 455, 574
Finley D., 1996. In: Bowyer S., Malina R.F. (eds.), Astrophysics in the Extreme Ultraviolet, Kluwer, Dordrecht, p. 223
Finley D., Koester D., Basri G., 1997, ApJ, in press
Holberg J.B., Barstow M.A., Buckley D.A.H., et al., 1993, ApJ 416, 806
Holberg J.B., Hubeny I., Barstow M.A., et al., 1994, ApJ 425, L105
Holberg J.B., Barstow M.A., Lanz T., Hubeny I., 1997, ApJ 484, 871
Jordan S., Koester D., Wulf-Mathies C., Brunner H., 1987, A&A 185, 253
Jordan S., Wolff B., Koester D., Napiwotzki R., 1994, A&A 290, 834
Jordan S., Finley D., Koester D., Wolff B., 1996. In: Zimmermann H.U., Trümper J.E., Yorke H. (eds.), Röntgenstrahlung from the Universe, MPE Report 263, Garching, p. 5
Jordan S., Koester D., Finley D., 1997a. In: Isern J., Hernanz M., Garcia-Berro E. (eds.), White Dwarfs, Kluwer, Dordrecht, p. 281
Jordan S., Wolff B., Finley D., Koester D., 1997b, A&A, in preperation
Kahn S.M., Wesemael F., Liebert J. et al., 1984, ApJ 278, 255
Koester D., 1989, ApJ 342, 999
Koester D., 1996. In: Bowyer S., Malina R.F. (eds.), Astrophysics in the Extreme Ultraviolet, Kluwer, Dordrecht, p. 185
Koester D., Wolff B., Jordan S., Dreizler S., 1997. In: Proceedings of the Third Conference on Faint Blue Stars, in press
Kurucz R.L., 1991. In: Crivellari L., Hubeny I., Hummer D.G. (eds.), Stellar Atmospheres: Beyond Classical Methods, p. 441
Lanz T., Barstow M.A., Hubeny I., Holberg J.B., 1996, ApJ 473, 1089
Marsh M.C., Barstow M.A., Buckley D.A., et al., 1997, MNRAS 287, 705
Paerels F.B.S., Heise J., 1989, ApJ 339, 1000
Petre R., Shipman H.L., Canizares C.R., 1986, ApJ 304, 356
Pradhan A.K., 1996. In: Bowyer S., Malina R.F. (eds.), Astrophysics in the Extreme Ultraviolet, Kluwer, Dordrecht, p. 569
Reid N., Wegner G., 1988, ApJ 335, 953
Rumph T., Bowyer S., Vennes S., 1994, AJ 107, 2108

Seaton M.J., Zeipper C.J., Tully J.A., et al., 1992, Rev.Mexicana Astron.Astrofiz., 23, 19
Vauclair G., Vauclair S., Greenstein J.L., 1979, A&A 80, 79
Vennes S., Fontaine G., 1992, ApJ 401, 288
Vennes S., Chayer P., Fontaine G., Wesemael F., 1989, ApJ 336, L25
Vennes S., Thejll P.A., Shipman H.L,1991. In: Vauclair G., Sion E. (eds.), White Dwarfs, Kluwer, Dordrecht, p. 235
Vennes S., Thejll P.A., Wickramasinghe D.T., Bessell M.S., 1996a, ApJ 467, 782
Vennes S., Chayer P., Hurwitz M., Bowyer S., 1996b, ApJ 468, 898
Vennes S., Thejll P.A., Génova Galvan R., Dupuis J., 1997, ApJ, in press
Vidal-Madjar A., Allard N.F., Koester D., et al., 1994, A&A 287, 175
Werner K., Dreizler S., 1994, A&A 286, L31
Werner K., Dreizler S., 1997. In: Kudritzki, Mihalas, Nomoto, Thielemann (eds.), Computational Astrophysics Vol. II, Springer, Berlin, in press
Wolff B., Jordan S., Koester D., 1996, A&A 307, 149
Wolff B., Koester D., Vidal-Madjar A., 1997. In: Isern J., Hernanz M., Garcia-Berro E. (eds.), White Dwarfs, Kluwer, Dordrecht, p. 199

This article was processed by the author using Springer-Verlag LaTeX A&A style file *L-AA* version 3.